Generalizing the correlated chromophore domain model of reversible photodegradation to include the effects of an applied electric field

Benjamin Anderson and Mark G. Kuzyk
Department of Physics and Astronomy, Washington State University, Pullman, Washington 99164-2814, USA
(Received 20 September 2013; revised manuscript received 21 January 2014; published 5 March 2014)

All observations of photodegradation and self-healing follow the predictions of the correlated chromophore domain model [Ramini *et al*., Polym. Chem. **4**, 4948 (2013)]. In the present work, we generalize the domain model to describe the effects of an electric field by including induced dipole interactions between molecules in a domain by means of a self-consistent field approach. This electric field correction is added to the statistical mechanical model to calculate the distribution of domains that are central to healing. Also included in the model are the dynamics due to the formation of an irreversibly damaged species, which we propose involves damage to the polymer mediated through energy transfer from a dopant molecule after absorbing a photon. As in previous studies, the model with one-dimensional domains best explains all experimental data of the population as a function of time, temperature, intensity, concentration, and now applied electric field. Though the precise nature of a domain is yet to be determined, the fact that only one-dimensional domain models are consistent with observations suggests that they might be made of correlated dye molecules along polymer chains. Furthermore, the voltage-dependent measurements suggest that the largest polarizability axis of the molecules are oriented perpendicular to the chain.

DOI: 10.1103/PhysRevE.89.032601 PACS number(s): 82.35.−x, 42.70.Jk, 81.05.Lg, 03.50.−z

I. INTRODUCTION

Organic dyes are widely used in many applications, such as liquid dye lasers [1–3], solid state dye lasers (SSDLs) [4–8], organic light-emitting diodes (OLEDs) [9,10], dye-sensitized solar cells (DSSCs) [11–17], fluorescence microscopy [18–21], and space-based optics [22–25]. As lasing media, organic dyes offer many advantages over other materials, as their broad absorption and emission peaks [26] allow for large tunability and generation of ultrashort pulses [27]. Additionally, organic dyes tend to have very large laser gains, making them a highly efficient lasing medium [28]. In the field of consumer electronics, OLEDs allow for the construction of extremely lightweight, ultrafast, and energy-efficient displays. Similarly, organic dyes in DSSCs offer the possibility of lightweight, inexpensive, and efficient solar cells [29–31]. Finally, organic dyes in fluorescence microscopy allow for high-resolution confocal imaging [19], three-dimensional imaging [20], and two-photon imaging [21].

While organic dyes offer many benefits over other materials, one fundamental hurdle is their photostability. Once degraded the dyes must be replaced, which in many applications is impractical, costly, and hazardous. To address the photostability of organic dyes, extensive work has focused on understanding and limiting the effects of photodegradation [12,13,16,22,32–54]. One method found to mitigate photodegradation of a dye is to dope it into a solid matrix such as a sol gel [46,47], silicate gel [48,49], or polymer [50,55,56]. Remarkably, in the case of some dye-doped polymers, photodegradation is not only mitigated, but is found to be completely reversible [55–59].

Reversible photodegradation is a relatively new phenomenon, with the first reported example being fluorescence decay and recovery of rhodamine and pyrromethene dye-doped polymer optical fibers [60]. Several years later the anthraquinone derivative 1-amino-2-methylanthraquinone (disperse orange 11 or DO11) doped into (poly)methyl-methacrylate (PMMA) was found to decay reversibly as probed by amplified spontaneous emission (ASE) [55–57]. Other anthraquinone derivatives have also been shown to exhibit self-healing [61], as well as 8-hydroxyquinoline aluminum (Alq) [62] and the octopolar molecule AF455 [58,59,63].

Photodegradation is generally an irreversible light-driven chemical reaction that produces new species, such as fragments of the original molecule. The formation of a new species is characterized by a change in the UV-visible (UV-VIS) absorption spectrum. In a two-component system in which molecules of one species (undamaged) are converted to a different (damaged) species, all spectra cross at an isosbestic point. DO11 molecules, the focus of our present studies, are found to photodegrade irreversibly in *liquid methyl-methacrylate* (MMA) monomer—as is typical for molecules in solution—with an isosbestic point in its UV-VIS absorption spectrum. In the *solid polymerized state* of MMA, i.e., PMMA polymer, the same experimental conditions show photodegradation with a similar isosbestic point [64], but the material subsequently recovers when the pump light is turned off. Thus the photodegradation pathway of the reversible process, as characterized by UV-VIS spectroscopy, appears to be of the same type as the irreversible process. Despite the term "photodegradation" typically implying irreversibility, since the decay pathway appears to be the same in both solution and polymer, we still call the reversible process *photodegradation*.

An argument may be made that the more complex structure of a polymer, with a distribution of chain lengths and inhomogeneity in rheological properties and composition, leads to transient processes that may mimic photodegradation and healing, but are in fact something different. However, since the spectra of what would be characterized as true photodegradation in liquid samples and in PMMA are similar suggests that the origins of the degradation processes are related, but with degradation in PMMA also exhibiting a recovery process.

There are several possible processes that could mimic self-healing, with the dye molecules still remaining damaged, including: recovery due to polymer relaxation, orientational hole burning, and photothermally induced diffusion of dye molecules. However, we find experimental evidence discounting these mechanisms as valid explanations. In the case of recovery processes that rely on polymer relaxation, they are known to be accelerated at elevated temperature [65]. In contrast, the self-healing process slows at elevated temperature [64,66]. In the case of orientational hole burning, there should be a measurable change in linear dichroism due to decay and recovery, but experimentally there is no such observation [57]. For photothermally induced diffusion of dye molecules, the UV-VIS absorbance spectrum will not have an isosbestic point and the burned area should show visible signs of diffusion. Yet for reversible photodegradation we do observe an isosbestic point, and direct imaging of a burn line reveals the process to be inconsistent with diffusion [67]. In addition, the observed temperature dependence of healing is opposite to what would be expected for diffusion.

Self-healing, while observed in many systems, is not universal and seems to rely on interactions between particular combinations of polymers and dopants. Given the evidence, it may be a new phenomena that is not derivable from the same old suspects. In an effort to understands its origin, many experiments and theoretical models have been developed.

For example, Embaye *et al*. developed a simple two-species model [57] in which a pristine molecule is damaged by photoinduced tautomerization that forms semistable dimers rather than nonreacting molecular fragments. Recovery was proposed to be in the dissociation of dimers back into single molecules. While Embaye's two-species model fits most experimental data at fixed temperature, concentration, and applied electric field, the theory's parameters do not predict the temperature, concentration, and applied electric field dependence, and so does not lead to any insights into the mechanism of healing.

To model temperature- and concentration-dependent reversible photodegradation of ASE in DO11/PMMA, Ramini *et al*. developed a correlated chromophore domain model (CCDM) [64] in which the dye molecules form correlated domains that foster the interaction between molecules, which promotes self-healing. From the experimental data the domains are found to be isodesmic (binding energy independent of domain size), which is typically only true for linear arrays of molecules [68–74]. The CCDM model assumes that healing is mediated by neighboring molecules, so the recovery rate increases in proportion to the domain size. At higher temperature, the average domain size decreases, inhibiting healing, thus explaining the observed decrease in recovery rate.

The CCDM was formulated based on a determination of the population of undamaged molecules using ASE experiments as a function of temperature and concentration, but due to experimental constraints could only be tested for a limited range of fluences. Simulations using the CCDM predict a strong dependence of the recovery rate on the fluence. However, linear transmittance measurements with fluences ranging over several orders of magnitude find the recovery rate to be constant as a function of fluence [61,75]. To reconcile the CCDM with this data, the CCDM's recovery dynamics were modified to include the effects of the damaged species in a domain. This modified model was found to be in agreement—within a constant offset—with linear transmittance measurements [66]. The constant offset [61,75–78] is attributed to an irreversibly damaged species not measurable by ASE. In contrast, transmittance is sensitive to both.

While the latest CCDM model [66] predicts the behavior of a broad range of experimental data, the nature of a domain remains elusive. The concept of the domain as the critical ingredient to the recovery process was introduced into the model because it works. Should domains not be responsible for the healing process, the mathematical structure of the correct theory would necessarily be the same.

Validation of a theory built on data from a given space of parameters requires the theory to be extended to an orthogonal space, and the predictions of the generalized theory to be tested in the new space. In this paper, we extend the model to include the effects of an electric field on a domain and test the model's predictions with electric-field-dependent experiments.

Recent measurements have shown that an applied electric field affects the photodegradation and recovery process [76–78]. In particular, applying a constant electric field during photodegradation and recovery has been shown to

(1) decrease the decay rate,
(2) decrease the amount of damage,
(3) decrease the recovery rate, and
(4) increase the recovery fraction.

The purpose of this work is to extend the CCDM using a self-consistent local field model of molecular interactions to take into account the effect of an electric field on domain size, and to test the predictions of this domain-based model on the new observations. Since the measurements are of samples exposed to high doses of light, an irreversible decay product is also formed. To take this into account, we include the effects of an irreversibly damaged species in the model. This generalized model is found to predict the observed effect of an electric field on reversible photodegradation. As such, we will see that the domain continues to be the common factor in all models that predict the observed behavior.

II. MODEL

A. Extension of domain model to include three species

The domain model of reversible photodegradation was initially developed using data obtained from ASE measurements in which only two species appear to be present—an undamaged species and a reversibly damaged species [64,66,79–81]. However, measurements using linear-optical transmittance techniques, such as transmittance imaging and absorbance spectroscopy, have shown that during decay a third species is formed which does not recover. [61,75–78].

To explain the irreversible species, which linear measurements observe but nonlinear measurements do not, we consider the nature of the two types of measurements. Nonlinear measurements primarily probe the dyes, as PMMA has a negligible nonlinear susceptibility. Linear optical measurements, on the other hand, measure both the dye's and polymer's optical properties. We therefore hypothesize that the irreversibly

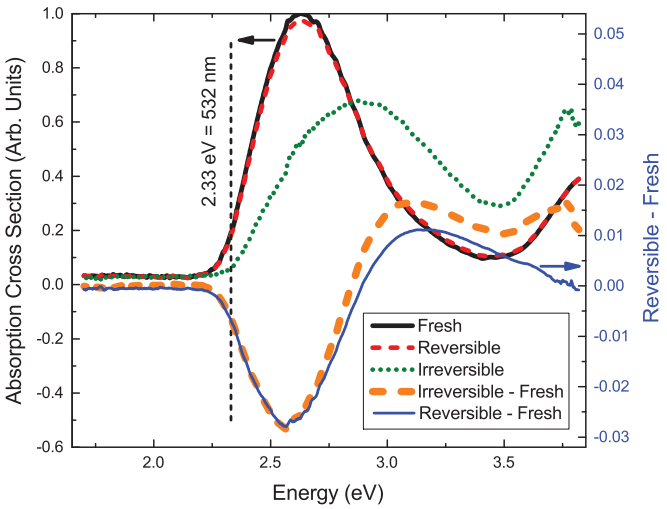

FIG. 1. (Color online) The absorption cross sections of the species involved in reversible and irreversible photodegradation. Also shown are the differences between the spectra.

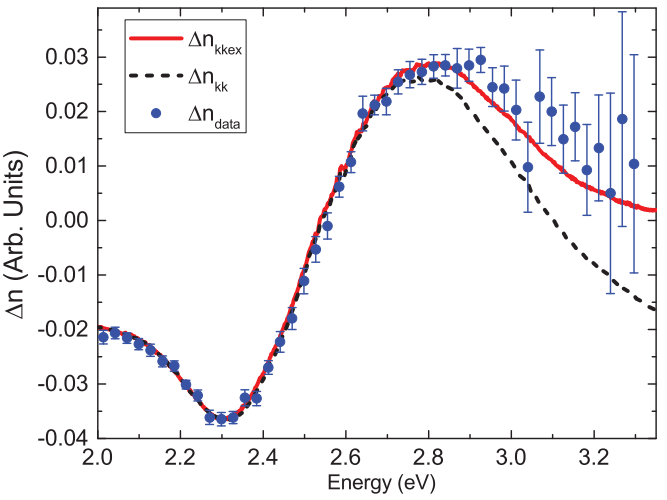

FIG. 2. (Color online) Change in refractive index during photodamage (points) and Kramers-Kronig transform of the absorption spectrum (dashed curve). The solid curve is generated by introducing a peak in the UV part of the spectrum to model the effects of polymer damage.

damaged species involve photodamage of the polymer, with the reversibly damaged species being related to damaged dye that does not yield ASE.

Figure 1 shows the absorption cross sections of the undamaged molecules (thick curve), the healing species (thin dashed curve), and the nonrecovering species (dotted curve). The spectrum of the undamaged molecules is determined from the absorption spectrum of a fresh sample. After heavy photodamage, the absorption spectrum contains all three species, while after recovery, the healing species is absent. These three measurements together can be used to determine the absorption cross section of each species [82], as shown in Fig. 1. The dashed vertical line at 2.33 eV (532 nm) labels the pump photon energy. Also shown are the differences between the fresh sample and both the reversible (thin curve) and irreversible (thick dashed curve) species. DO11 molecules and the reversible decay products both absorb the pump light about equally and more strongly than the irreversible species.

Two-photon absorption measurements of AF455 dyes in PMMA polymer [58,58] and ASE measurements of DO11 dye in PMMA polymer [57] both show decay in signal and recovery, implying that the pristine molecules produce the signal and the damaged species produce little or no signal. The neat polymer produces no signal in both cases. In contrast, the change in the absorption spectrum as shown in Fig. 1 is small during degradation, but both species have a similar difference spectrum relative to the undamaged molecule, though the magnitude of the change for the irreversible species is about 20 times greater than the reversible species. In addition, the two curves match on the low-energy side of the dip but diverge by an ever-greater amount on the high-energy side. This data suggests that perhaps the changes to the molecular structure are similar in both cases, but to a much higher degree in the irreversible case where perhaps the polymer plays a greater role.

The change in refractive index when pumping the sample with high enough intensity to produce a large population of the irreversible species gives one more crucial piece of information about the irreversible species. Figure 2 shows the change in refractive index (points) as determined with a white-light interferometer microscope (WLIM) after damage [83]. The dashed curve shows the predicted refractive index change from a Kramers-Kronig transformation of the measured change in absorbance. The solid curve shows the change in refractive index when a peak is added in the UV part of the spectrum to mimic the effect of damaged PMMA. With this peak added, the data matches the theory and is consistent with the hypothesis that the polymer is involved.

Thus the reversible process is most likely one in which a molecule is damaged into a form that does not produce an ASE signal and then recovers back to its original form, which does emit ASE. Since nonlinear measurements show only the reversible process, the irreversible process either produces molecular fragments that are not observed with ASE or irreversible polymer damage is also involved. Note that above a fluence threshold, nonlinear measurements detect irreversibility, implying that the dye molecules can also be irreversibly damaged, but all measurements reported here are well below that threshold.

Taking all of these observations together, we assume that irreversible decay occurs simultaneously with reversible decay, i.e., the decay channels are parallel. A schematic representation of this process is shown in Fig. 3, where the undamaged molecules absorb light and either decay into the reversible species or the irreversible species. Mathematically, this system is modeled by three rate equations:

$$\frac{dn_0}{dt} = -\left(\frac{\alpha}{N} + \epsilon N\right) I n_0 + \beta N n_1, \tag{1}$$

$$\frac{dn_1}{dt} = \frac{\alpha I}{N} n_0 - (\beta + \underline{\underline{\epsilon I}}) N n_1, \tag{2}$$

$$\frac{dn_2}{dt} = \epsilon N I (n_0 + \underline{\underline{n_1}}), \tag{3}$$

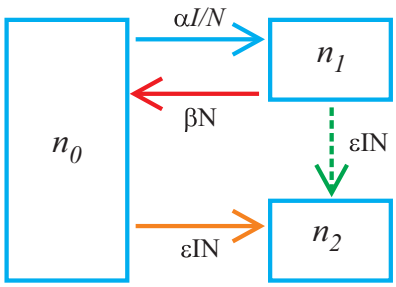

FIG. 3. (Color online) Schematic diagram of the three-species process. The decay processes occur in parallel, but only one species recovers.

where N is the domain size, α is the intensity-independent decay rate of the reversible decay process, ϵ is the intensity-independent decay rate of the irreversible process, β is the recovery rate, and I is the intensity. The domain size dependence of both the reversible decay rate ($\frac{\alpha}{N}$) and the recovery rate (βN) are retained from Ramini's CCDM [66], and the domain size dependence of the irreversible decay rate is chosen to match experimental observations with linear transmittance imaging [61,75,76,84]. An ensemble average of Eqs. (1)–(3) over the distribution of domain sizes, as described by Ramini *et al.* [64,66], yields the macroscopic properties.

The terms with double underlines in Eqs. (2) and (3) are represented by the dashed arrow in Fig. 3. Models with and without these two terms both fit the data. Their meaning is described below.

There are several possible mechanisms for irreversible degradation of the polymer host. First, light absorption by the dye can lead to energy transfer to the polymer, resulting in irreversible damage. Second, light absorbed by the dyes produces free ions or radicals which interact with the polymer chain, forming either singlet oxygen [35,36,39,42] and/or electron donor-acceptor complexes [43,85]. The singlet oxygen and/or electron donor-acceptor complexes can then produce irreversible chemical reactions, including hydrogen abstraction [35,44,45], carbonyl group formation [42,86], hydroperoxide formation [87], and/or other reactions [35]. Independent of the mechanism of polymer damage, it will become greater as the dye concentration is increased, which is represented by an intensity-independent decay rate in proportion to ϵN.

The spectrum of the reversible and irreversible species are similar. If energy transfer from the dye to the polymer is responsible for irreversible damage, then both should result in the same amount of damage. The underlined term in Eq. (3) represents irreversible damage due to energy transfer to the polymer from the reversible species. The molecule that mediates energy transfer need not be depleted, but could in principle act as a catalyst. If this were true, then the term with the ϵ factor in Eqs. (1) and (2) would be absent. The absorption spectra of the irreversible species shown in Fig. 1 is different than the other two, implying that populations n_0 and n_1 are used up in the process when the polymer is damaged. The refractive index change in the UV part of the spectrum signals damage to the polymer, so perhaps the damaged species is a complex made of a damaged molecule associated with damaged polymer. Both models (with and without the underlined terms) fit the data because those terms are small. A broader range of intensities will need to be measured in order to differentiate between the two models.

There are two important points that need to be made here about the irreversible degradation product. First, it must be taken into account because the linear absorption spectroscopy measurements used in characterizing the material measures its contribution. Nonlinear-optical measurements, though more sensitive and selective, are more noisy and measure a smaller dynamic range of population fraction, so are not used in the present work. Second, if the polymer is involved in domain formation of dopant molecules, the measured damage to the polymer may shed light on the nature of the domains. This type of analysis is beyond the scope of this paper, but we briefly describe it here to place our work in broader perspective.

Given the hypothesis that the irreversible species is related to polymer damage, the domain size dependence of Eq. (3) may be understood as relating to the coupling of dye and polymer. Since the neat PMMA absorption cross section peaks in the UV, a dye that absorbs photons in the visible and transfers the energy to the polymer will power the degradation process in the polymer. As the local concentration of dye molecules increases, the likelihood of an absorbed photon that leads to polymer damage increases. This relationship is consistent with the irreversible decay rate being proportional to domain size.

The picture above is consistent with observations that under standard photodegradation experimental conditions, neat PMMA shows no appreciable change in its absorption spectrum. However, when dyes are added to the PMMA in solid solution, a degradation product is formed.

To solve for the population dynamics, Eqs. (1)–(3) are written in matrix form as

$$\frac{d\mathbf{x}}{dt} = \xi \mathbf{x}, \tag{4}$$

where the column vector $\mathbf{x} = (n_0, n_1, n_2)$ and the matrix ξ is

$$\xi = \begin{pmatrix} -\left(\frac{\alpha}{N} + \epsilon N\right) I & \beta N & 0 \\ \frac{\alpha}{N} I & -\beta N & 0 \\ \epsilon N I & 0 & 0 \end{pmatrix}. \tag{5}$$

The general solution to Eq. (4) is

$$\mathbf{x} = c_0 \mathbf{v}_0 e^{\lambda_0 t} + c_1 \mathbf{v}_1 e^{\lambda_1 t} + c_2 \mathbf{v}_2 e^{\lambda_2 t}, \tag{6}$$

where λ_i are the eigenvalues of ξ, $\mathbf{v}_i$ are the eigenvectors, and c_i are constants found from the initial conditions. To simplify the form of the eigenvalues and eigenvectors, we define three parameters:

$$A = \beta N + \left(\frac{\alpha}{N} + \epsilon N\right) I, \tag{7}$$

$$C = \beta N + \left(\frac{\alpha}{N} - \epsilon N\right) I, \tag{8}$$

$$B = \sqrt{-4\beta\epsilon N^2 I + \left[\beta N + \left(\frac{\alpha}{N} + \epsilon N\right) I\right]^2}. \tag{9}$$

The eigenvalues are then given by

$$\lambda_0 = 0, \tag{10}$$

$$\lambda_1 = \frac{-A-B}{2}, \tag{11}$$

$$\lambda_2 = \frac{-A+B}{2}, \tag{12}$$

and the eigenvectors are

$$\mathbf{v}_0 = \begin{pmatrix} 0 \\ 0 \\ 1 \end{pmatrix} \quad \mathbf{v}_1 = \frac{1}{2\epsilon NI}\begin{pmatrix} -A-B \\ C+B \\ 2\epsilon NI \end{pmatrix}, \tag{13}$$

$$\mathbf{v}_2 = \frac{1}{2\epsilon NI}\begin{pmatrix} -A+B \\ C-B \\ 2\epsilon NI \end{pmatrix}. \tag{14}$$

Assuming the system is initially undamaged, the population dynamics of a domain of size N are

$$n_0(t) = \frac{1}{2B(A-C)} e^{-\frac{1}{2}(A+B)t}((A+B)(B-C) + (A-B)(B+C)e^{Bt}), \tag{15}$$

$$n_1(t) = \frac{(B-C)(B+C)e^{-\frac{1}{2}(A+B)t}(-1+e^{Bt})}{2B(A-C)}, \tag{16}$$

and

$$n_2(t) = -\frac{\epsilon NI}{B(A-C)} e^{-\frac{1}{2}(A+B)t}[C(-1+e^{Bt}) + B(1+e^{Bt}-2e^{\frac{1}{2}(A+B)t})]. \tag{17}$$

Equations (15)–(17) are the population dynamics for a single domain, where the macroscopic dynamics are an ensemble average over a distribution of domains size N, $\Omega(N)$. Using an isodesmic aggregation model, Ramini *et al.* derived the distribution of domains of size N to be of the form [64,66]

$$\Omega(N) = \frac{1}{z}\left[\frac{(1+2\rho z) - \sqrt{1+4\rho z}}{2\rho z}\right]^N, \tag{18}$$

where $\Omega(N)$ is the distribution function, $z = \exp(\mu/kT)$, ρ is the total number of molecules in a given volume, and μ is the free energy advantage of having a molecule being in a domain versus outside of a domain.

The free energy advantage is found by comparing the energy of a domain size N to the energy of a free molecule and a domain of size $N-1$,

$$\mu = E(N) - [E(N-1) + E(1)], \tag{19}$$

where $E(N)$ is the energy of a domain of size N, and $E(N-1)+E(1)$ is the energy of a domain of size $N-1$ and a single molecule outside of the domain. The free energy advantage due to aggregation alone is defined to be λ [64,66]. The following section presents a model that takes into account the effect of an electric field on the free energy advantage.

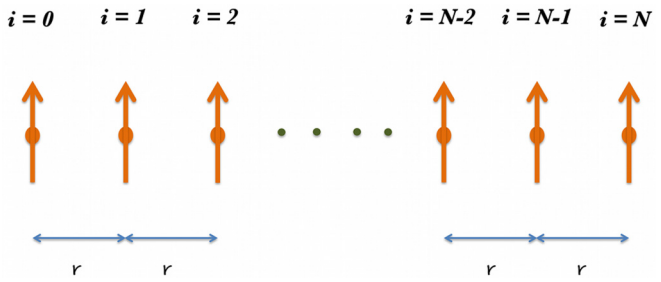

FIG. 4. (Color online) Diagram of model system geometry of N equally spaced point dipole molecules.

B. Effect of an electric field on the distribution of domains

To model the effect of an applied electric field E_0 on the distribution of domains, we consider the change in free energy advantage due to the field. Our dielectric model, which is an extension of Ramini's model, assumes that a domain is a linear array of equally spaced point molecules each having polarizability α and with the induced dipole moment along the applied field, as shown in Fig. 4.

In the dilute case, the molecules are essentially noninteracting, and the total dipole moment of the domain is

$$P = \sum_{i=1}^{N} p_i, \tag{20}$$

$$= N\alpha E_0, \tag{21}$$

where N is the size of the domain and p_i is the dipole moment of the ith molecule in the domain. Additionally, the total dielectric energy of the domain is

$$U(N) = -N\alpha E_L^2, \tag{22}$$

$$= -N\alpha E_0^2, \tag{23}$$

where $E_L = LE_0$ is the local electric field, with $L = 1$ being the local field factor for the noninteracting case. Substituting Eq. (23) into Eq. (19), with $E(N) \to E(N) + U(N)$, yields $\mu = \lambda$; thus in the noninteracting case there is no change in the distribution of domains due to the application of an applied electric field.

To account for dielectric interactions between molecules in a domain, we assume that each molecule behaves as a point dipole, and the field from all other dipoles contributes to the local field. To solve this system we use a self-consistent field model, similar to Dawson *et al.* [88,89]. Assuming that the interactions occur only between molecules in the same domain, we can write the dipole moment of the ith molecule in a domain as

$$p_i = \alpha\left[E_0 - \sum_{j=1}^{i-1}\frac{p_j}{[(i-j)r]^3} - \sum_{j=i+1}^{N}\frac{p_j}{[(j-i)r]^3}\right], \tag{24}$$

where the effect of the other molecules in the domain is to decrease the local field experienced by the ith molecule. The total dipole moment of the domain is found by summing over

the dipole moments of every molecule in the domain,

$$P = \sum_{i=1}^{N} p_i, \tag{25}$$

$$= N\alpha E_0 - \sum_{i=1}^{N}\sum_{j\neq i}^{N} \frac{p_j}{(|i-j|r)^3}. \tag{26}$$

To find the individual dipole moments we can rewrite Eq. (24) as a matrix equation,

$$\mathbf{P} = \alpha E_0 \mathbf{1} - \frac{\alpha}{r^3}\mathbf{M}\mathbf{P}, \tag{27}$$

where the column vector $\mathbf{P} = \{p_1, p_2, \ldots, p_N\}$, the column vector $\mathbf{1} = \{1,1,\ldots,1\}$, and $\mathbf{M}$ is an $N \times N$ matrix with elements given by

$$M_{ij} = \begin{cases} 0 & \text{if} \quad i = j \\ \frac{1}{|i-j|^3} & \text{if} \quad i \neq j \end{cases}. \tag{28}$$

Solving for $\mathbf{P}$ we obtain

$$\mathbf{P} = \alpha E_0 \left(\mathbf{I} + \frac{\alpha}{r^3}\mathbf{M}\right)^{-1} \mathbf{1}, \tag{29}$$

where $\mathbf{I}$ is the identity matrix, and the superscript -1 denotes the matrix inverse.

It is beyond the scope of this paper to present a comprehensive solution to Eq. (29). Instead, we consider the total dipole moment of a domain in the case where $\alpha \ll r^3$, which is given by

$$P(N) \approx N\alpha E_0 - 2\zeta(3)(N-1)\frac{\alpha^2}{r^3}E_0, \tag{30}$$

$$= N\alpha L(N) E_0, \tag{31}$$

where ζ is the ζ function, with $\zeta(3) \approx 1.202$, and L is the local field factor given by

$$L(N) = 1 - \frac{2\zeta(3)(N-1)}{N}\frac{\alpha}{r^3}. \tag{32}$$

Substituting Eq. (32) into Eq. (22) the dielectric energy for a domain of size N including first-order interactions is

$$U(N) = -N\alpha L(N)^2 E_0^2, \tag{33}$$

$$\approx -N\alpha E_0^2 + 4\zeta(3)(N-1)\frac{\alpha^2}{r^3}E_0^2, \tag{34}$$

where terms proportional to α^2/r^6 are again neglected.

With the dielectric energy of a domain size N and the aggregation energy used by Ramini *et.al*, $E = -\lambda(N-1)$ [64,66], the total energy of a domain is:

$$E(N) = -\lambda(N-1) - N\alpha E_0^2 + 4\zeta(3)(N-1)\frac{\alpha^2}{r^3}E_0^2. \tag{35}$$

Substituting Eq. (35) into Eq. (19), we find the free energy advantage, including dielectric effects, to be

$$\mu = \lambda - \frac{4\zeta(3)\alpha^2}{r^3}E_0^2. \tag{36}$$

Therefore, with an applied electric field, the z parameter in Eq. (18) becomes

$$z = \exp\left\{\frac{\mu}{kT}\right\}, \tag{37}$$

$$= \exp\left\{\frac{\lambda}{kT} - \frac{4\zeta(3)\alpha^2}{kTr^3}E_0^2\right\}, \tag{38}$$

$$= \exp\left\{\gamma - \eta E_0^2\right\}, \tag{39}$$

where $\gamma = \frac{\lambda}{kT}$ and $\eta = \frac{4\zeta(3)\alpha^2}{kTr^3}$.

While the dielectric model is simplistic and does not account for finite-sized molecules that are distributed unequally in three dimensions, we find that the model contains the essential physics describing the system: an applied electric field induces a dipole field which acts to decrease the free energy advantage of the system and causes the domains to dissociate. While the model is not precise given its simplistic geometry, as we later show, it correctly predicts the measured functional dependence of the free energy advantage on domain size and applied electric field. We note that this model implicitly assumes that the induced dipole moment is perpendicular to the one-dimensional chain. If the induced dipoles were aligned along the chain, the applied electric field would induce an attractive force between the molecules, leading to increased domain size. Thus the voltage-dependent data yields information on molecular alignment, as discussed later.

C. Integrated model

Linear-optical measurements do not directly measure the three species. Instead, they probe a linear combination weighted by spectral properties of each species. In the approximation of a thin sample, such that the pump intensity is constant as a function of depth, the absorbance A may be written as

$$A = \overline{n}_0(t)\sigma_0 L + \overline{n}_1(t)\sigma_1 L + \overline{n}_2(t)\sigma_2 L, \tag{40}$$

where L is the sample thickness, σ_i is the absorbance cross section for the i^{th} species, and the populations $\overline{n}_i$ are the ensemble averages over the distribution of domains given by

$$\overline{n}_0(t) = \sum_{N=1}^{\infty} n_0(N,t)\Omega(N), \tag{41}$$

$$\overline{n}_1(t) = \sum_{N=1}^{\infty} n_1(N,t)\Omega(N), \tag{42}$$

$$\overline{n}_2(t) = \sum_{N=1}^{\infty} n_2(N,t)\Omega(N), \tag{43}$$

where $n_i(N,t)$ are given by Eqs. (15)–(17), and the distribution of domains $\Omega(N)$ is given by Eq. (18).

Assuming that the region of interest is originally undamaged, the change in absorbance due to photodegradation is

$$\Delta A = \overline{n}_1(t)(\sigma_1 - \sigma_0)L + \overline{n}_2(t)(\sigma_2 - \sigma_0)L, \tag{44}$$

$$= \overline{n}_1(t)\Delta\sigma_1 L + \overline{n}_2(t)\Delta\sigma_2 L, \tag{45}$$

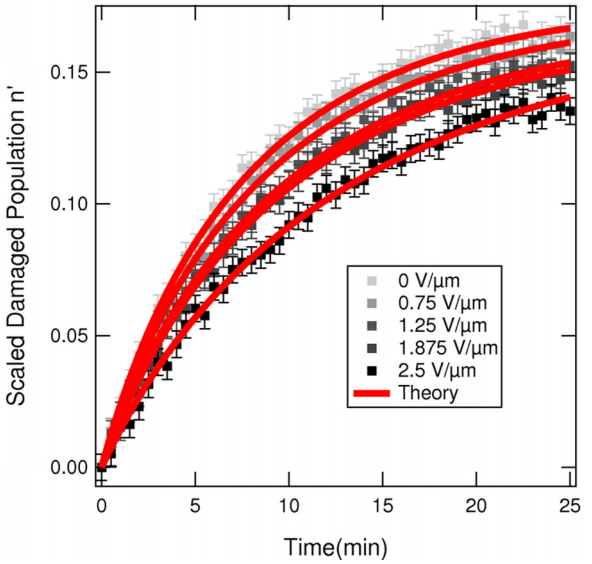

FIG. 5. (Color online) Decay of scaled damaged population as a function of time (points) for different applied fields for an intensity of 175 W/cm^2, and theory (curves).

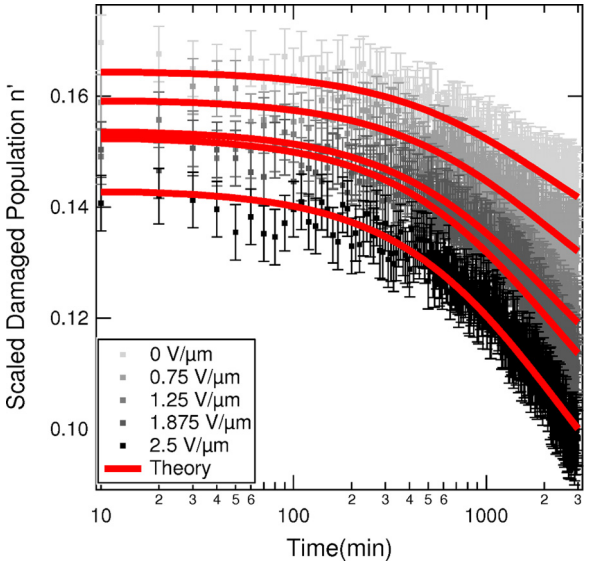

FIG. 6. (Color online) Recovery of scaled damaged population as a function of time (points) for different applied fields after a 25-min burn of 175 W/cm^2 intensity, and theory (curves).

where $\Delta\sigma_i = \sigma_i - \sigma_0$. For consistency with our previous papers [61,75–78], we label ΔA as the scaled damaged population n' which is proportional to the combined damaged population of both damaged species.

III. RESULTS

To test the extended correlated chromophore domain model (eCCDM) we use data from our previous study of electric-field-dependent reversible photodegradation [78]. The data set consists of the scaled damaged population at the burn center during decay and recovery, as well as the reversible and irreversible amplitudes found at a wide range of intensities. Each measurement is repeated for five different applied electric field strengths with the polarity of the applied field held constant throughout all testing. The theory is fit to the full data set with one adjustable parameter, which accounts for point-to-point variations in the sample.

Figures 5 and 6 show the scaled damage population during decay and recovery, respectively, for the pump beam center, which has an intensity of 175 W/cm^2. Using points along the pump beam profile as samples of different intensity, we fit the scaled damage population during recovery as a function of time using an exponential fit,

$$n' = n'_{IR} + n'_R e^{-\beta t}, \tag{46}$$

where the exponential offset n_{IR} is proportional to the irreversibly damaged population formed during photodegradation, and the exponential amplitude n_R is proportional to the reversibly damaged population remaining right after degradation.

To determine the dynamics of the reversible species, the permanently damaged population must be removed using Eq. (46). Figure 7 shows a log plot of the residual after the permanently damaged species is subtracted from the data in Fig. 7. The recovery rate of the reversible population is proportional to the slope of the lines, so as the field strength is increased the recovery rate decreases.

Figure 8 shows the exponential amplitude as a function of intensity, and Fig. 9 shows the exponential offset as a function of intensity. While the full data set is used for fitting, Figs. 8 and 9 only show smoothed data for three field strengths, as the raw data is extremely noisy due to point-to-point variations caused by sample inhomogeneity.

To test the eCCDM, the full data set is fit to Eq. (45), with the model parameters α, β, ϵ, ρ, λ, and η being held constant for all fits. Only the amplitude factors in Eq. (45),

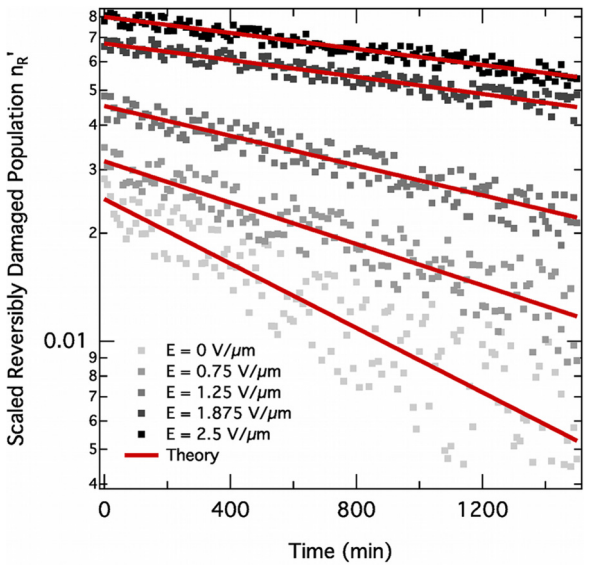

FIG. 7. (Color online) Conversion of the scaled population of only the reversible component into the original species, determined by subtracting the permanently damaged population according to Eq. (46).

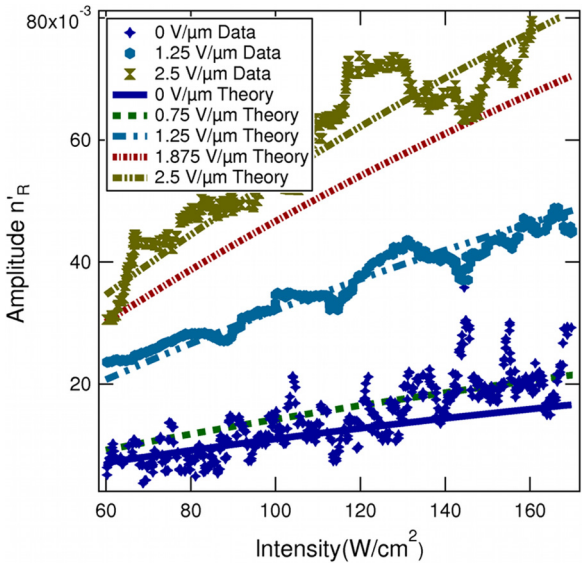

FIG. 8. (Color online) Measured amplitude of recovered population as a function of intensity (points) and theory (curves). The amplitude scales with the reversibly damaged population n_1 [Eq. (16)]. Fits for each field strength are displayed, but smoothed data is shown for only three representative field strengths to avoid clutter.

$\Delta\sigma_1 L$ and $\Delta\sigma_2 L$, are allowed to vary from fit to fit to account for sample inhomogeneity. Table I tabulates the model parameters found from fitting the full data set. To compare the results of the eCCDM to the previous CCDM, we include the domain parameters (ρ and λ), found previously using ASE as a probe [64,66]. However, since the models contain different numbers of species, we are unable to directly compare the rate parameters.

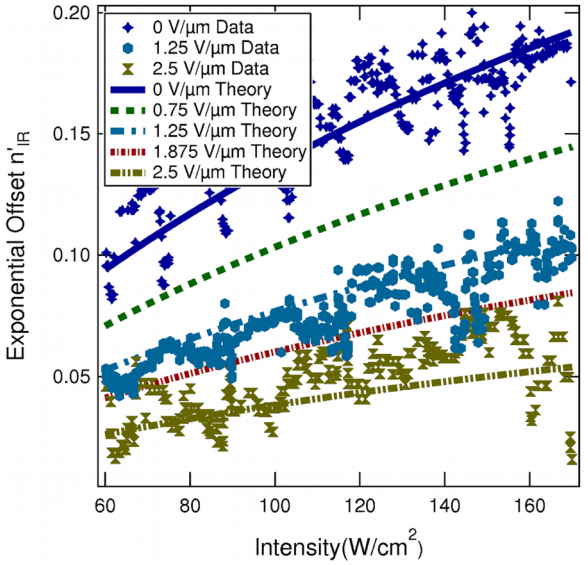

FIG. 9. (Color online) Offset (n'_{IR}) in recovery data. Plots of the offset as a function of intensity are shown (points) with theory (curves). Population of irreversibly damaged species n_2 [Eq. (17)], formed during decay, is manifested in an offset n_{IR}. Fits for each field strength are displayed, but smoothed data is shown for only three representative field strengths to avoid clutter.

TABLE I. Model parameters for the eCCDM found from electric-field-dependent reversible photodegradation measurements. The thermodynamic quantities, ρ and λ, are compared to previous measurements [64,66].

Parameter	New	Old
α (10^{-2} cm^2/(W min))	1.32($\pm$0.33)	–
β (10^{-5} min^{-1})	2.53($\pm$0.51)	–
ϵ (10^{-6} cm^2/(W min))	6.47($\pm$0.21)	–
ρ (10^{-2})	1.19($\pm$0.25)	1.2($\pm$0.2)
λ (eV)	0.29($\pm$0.02)	0.29($\pm$0.01)
η (10^{-14} m^2 V^{-2})	2.210($\pm$0.070)	–

IV. DISCUSSION

The dopant molecules are anisotropic, so the polarizability is largest along one principle axis, call it x, and smaller along the other principle axis, y. For the sake of argument, we assume the molecule has azimuthal symmetry about x, but this does not change the more general argument.

Consider the case where the molecular x axis is locally perpendicular to the chain that defines the one-dimensional domain. If the chains are randomly aligned, then the field will be (1) approximately along x for some contiguous subset of molecules and (2) along y for another contiguous subset of molecules. In those sections where the field is along x, the resulting repulsive forces will break up domains, and in those sections where the field is along y, the force will be attractive and molecules will be attracted to the domain. Because the polarizability is larger along x, the number of molecules that break away from a domain exceeds the number that are attracted to the domain. As such, the average domain size decreases.

If the molecular y axis, the one with smaller polarizability, is perpendicular to the chain, the average domain size will grow. If the molecule is isotropic, then the two competing effects will balance and the electric field will not have an effect on the photodegradation and recovery time constants.

The DO11 molecule is more complex, with three distinct polarizabilities. Nevertheless, side-by-side molecules with parallel dipole moments will repel and the end-to-end configuration will lead to attraction. Even with an idealized molecule, there is no guarantee that they will be parallel or perpendicular, but rather will be described by an orientational distribution function. In addition, the molecules may on average be tilted relative to the chain.

Independent of these complications, if the projection of the polarizability perpendicular to the chain is larger than parallel, the behavior that we calculate will be obeyed and the strength of the effect will be related to the order parameter that describes the alignment between the molecular distribution and the chain. As such, the voltage-dependent measurement differentiates between these two cases. We thus conclude that the data strongly suggests that the domains are made of molecules that are oriented approximately perpendicular to the chain.

The previous section shows that the eCCDM accurately describes transmittance imaging data as a function of time, intensity, and applied electric field. However, the underlying

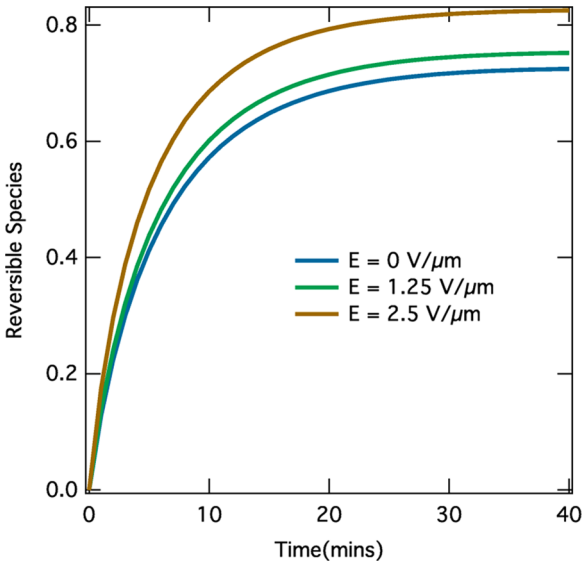

FIG. 10. (Color online) Population of reversibly damaged species as a function of time during photodegradation. Curves are calculated using one set of fit parameters for three applied field strengths.

population dynamics are masked, as the scaled damaged population is a linear superposition of both damaged species. Therefore, using the model parameters in Table I, we determine the underlying population dynamics. Figure 10 shows the reversibly decayed species as a function of time during decay for three field strengths, and Fig. 11 shows the irreversibly decayed species during decay for three field strengths.

As the applied field is increased, more of the reversibly damaged population is produced and at a faster rate. On the other hand, with increasing field strength, less of the irreversibly damaged population is formed and at a slower rate.

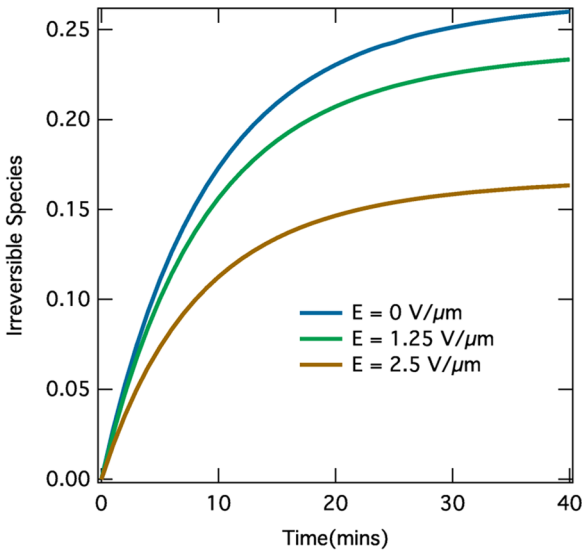

FIG. 11. (Color online) Population of irreversibly damaged species as a function of time during photodegradation. Curves are calculated using one set of fit parameters for three applied field strengths.

This observation is opposite that of previous measurements of purely irreversible decay of dye-doped polymers under an applied electric field [90–92]. These results, coupled with previous measurements of temperature-dependent reversible photodegradation [64,66], suggest that the underlying mechanism of reversible photodegradation is unique.

A domain model assuming linear aggregates of correlated dye molecules fits all experimental data as a function of intensity, temperature, concentration, and applied electric field. In this model the dynamics of decay and recovery are governed by the distribution of domain sizes. A precise calculation of the effect of varying concentration, temperature, and/or electric field on population dynamics requires calculating the ensemble average in Eqs. (41)–(43). A more simple but approximate way to glean an understanding of the dynamics is to consider the average domain size as a function of temperature, concentration, and applied electric field.

The probability of a domain having size N is $P(N) = N\Omega(N)$. Therefore the average domain size is

$$\langle N\rangle = \frac{\sum_{N=1}^{\infty} NP(N)}{\sum_{N=1}^{\infty} P(N)}, \tag{47}$$

$$= \frac{1}{\rho z}\sum_{N=1}^{\infty} N^2 (z\Omega_1)^N, \tag{48}$$

$$= \frac{\Omega_1 (1 + z\Omega_1)}{\rho\,|z\Omega_1 - 1|^3}, \tag{49}$$

where $z = \exp\{\mu/kT\}$, $\rho = \sum_{N=1}^{\infty} P(N)$, and

$$\Omega_1 = \frac{(1 + 2\rho z) - \sqrt{1 + 4\rho z}}{2\rho z^2}. \tag{50}$$

Figure 12 shows the average domain size as a function of temperature and applied electric field for $\rho = 0.012$. As the temperature and/or applied field is increased, the average domain size decreases. This implies that the effect of an applied field and/or temperature increase is to break apart domains into smaller sizes.

To understand this effect, we recall that the free energy advantage μ is essentially a binding energy describing the

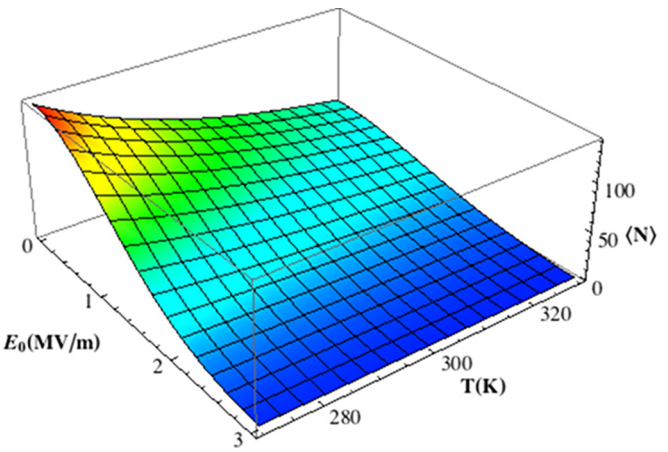

FIG. 12. (Color online) Average domain size as a function of temperature and applied electric field using parameters found from fits.

attachment of molecules to a domain. When increasing the applied electric field, the repulsive dipole-dipole interactions weaken the overall binding energy, making it easier for a molecule to break free of a domain. Additionally, when increasing the temperature, the greater thermal energy causes domains to break apart.

Despite the model's success, the nature of the domains is still unknown. Based on the following experimental/modeling evidence, we know that

(1) A dye must be in a polymer matrix to exhibit self-healing [55,56].

(2) Not only does the polymer mediate dye recovery, but dye can mediate polymer recovery [63].

(3) Molecules in a domain are protected from optical damage and self-healing is accelerated in proportion to the size of the domain [64,66].

(4) The irreversibly decayed species appears to be associated with polymer damage, suggesting that dye and polymer are both involved.

(5) Models of domain geometries other than linear aggregates have been tested and are found to be inconsistent with experimental data, so the domains are most likely one dimensional.

(6) The large polarization principle axis of each molecule in the domain is on average perpendicular to the chain.

We propose that domains consist of molecules correlated with each other through a single polymer chain. Currently the nature of how dyes and polymer chains form domains is under study, but given the measured domain binding energy of $\lambda = 0.29$ eV, Kuzyk and Ramini proposed a simple hydrogen bonding scheme between a DO11 tautomer and PMMA, which is of the same binding energy [80,81]. To further test this hypothesis, studies are underway that vary dye structure and polymer type, as these will change the binding energy if hydrogen bonding between the dye and polymer is responsible for domain formation. Additionally, we are using Fourier transform infrared, micro-Raman, and scattering in order to better understand the nature of domains.

V. CONCLUSIONS

Using a dielectric model of a linear array of equally spaced dipoles, we have extended the correlated chromophore domain model to account for the effects of an applied electric field on reversible photodegradation. The new model is observed to be consistent with all experiments in which an electric field is applied. As such, the domain appears to be the unifying factor.

The sign of the shift in binding energy in response to an applied electric field differentiates between parallel and perpendicular alignment with the chain. We find that the large polarizability axis is on average perpendicular to the chain. This result is the first step in determining the mechanisms for domain formation, which may lead to a better understanding of how domains promote self-healing.

In both the case of the aggregation energy λ and the electric-field-induced energy, the free energy advantage is found to be independent of domain size, suggesting linear aggregates [68–74]. Most likely these aggregates are molecules correlated with each other through a polymer chain. This picture is consistent with the hypothesis that the irreversible species is due to photoinduced damage to the polymer that is mediated by energy transfer from a dye upon photodegradation.

ACKNOWLEDGMENTS

We would like to thank Sheng-Ting Hung for help with sample preparation, as well as Wright Patterson Air Force Base and the Air Force Office of Scientific Research (FA9550-10-1-0286) for their continued support of this research.

[1] P. Sorokin and J. Lankard, IBM J. Res. Dev. **10**, 162 (1966).
[2] P. Sorokin and J. Lankard, IBM J. Res. Dev. **11**, 148 (1967).
[3] P. Sorokin, J. Lankard, E. Hammond, and V. Moruzzi, IBM J. Res. Dev. **11**, 130 (1967).
[4] B. Soffer and B. McFarland, Appl. Phys. Lett. **10**, 266 (1967).
[5] A. Maslyukov, S. Sokolov, M. Kaivola, K. Nyholm, and S. Popov, Appl. Opt. **34**, 1516 (1995).
[6] F. Duarte and R. James, Opt. Lett. **28**, 2088 (2003).
[7] A. Costela, I. Garcia-Moreno, and R. Sastre, *Tunable Laser Applications*, 2nd ed. (CRC Press, Boca Raton, FL, 2009), p. 97.
[8] F. Duarte and R. James, *Tunable Laser Applications*, 2nd ed. (CRC Press, Boca Raton, FL, 2009), p. 121.
[9] C. Tang and S. Vanslyke, Appl. Phys. Lett. **51**, 913 (1987).
[10] J. Burroughes, D. Bradley, A. Brown, R. Marks, K. Mackay, R. Friend, P. Burns, and A. Holmes, Nature (London) **347**, 539 (1990).
[11] H. Gerischer, M. Michel-Beyerle, E. Rebentrost, and H. Tributsch, Electrochim. Acta **13**, 1509 (1968).
[12] M. Matsumura, S. Matsudaira, H. Tsubomura, M. Takata, and H. Yanagida, Ind. Eng. Chem. Prod. Res. Dev. **19**, 415 (1980).
[13] M. Krunks, A. Katerski, T. Dedova, A. Mere, and I. O. Acik, US Patent No. 8,614,393 (24 December 2013).
[14] M. Liang and J. Chen, Chem. Soc. Rev. **42**, 3453 (2013).
[15] K. Hara and N. Koumura, Mater. Matters **4.4**, 92 (2009).
[16] H. Tributsch, Photochem. Photobiol. **16**, 261 (1972).
[17] Y. Wu, M. Marszalek, S. M. Zakeeruddin, Q. Zhang, H. Tian, M. Gratzel, and W. Zhu, Energy Environ. Sci. **5**, 8261 (2013).
[18] J. Lichtman and J. Conchello, Nat. Methods **2**, 910 (2005).
[19] Y. Dai, R. Whittal, and L. Li, Anal. Chem. **68**, 2494 (1996).
[20] D. Agard, Y. Hiraoka, P. Shaw, and J. Sedat, *Fluorescence Microscopy of Living Cells in Culture, Part B*, edited by Y.-L. Wang and D. Taylor, Methods in Cell Biology Vol. 30, (Academic Press, New York, 1989) p. 353.
[21] P. So, C. Dong, B. Masters, and K. Berland, Annu. Rev. Biomed. Eng. **2**, 399 (2000).

[22] E. W. Taylor, J. E. Nichter, F. D. Nash, F. Haas, A. A. Szep, R. J. Michalak, B. M. Flusche, P. R. Cook, T. A. McEwen, B. F. McKeon, P. M. Payson, G. A. Brost, A. R. Pirich, C. Castaneda, B. Tsap, and H. R. Fetterman, Appl. Phys. Lett. **86**, 201122 (2005).

[23] M. G. Kuzyk, E. W. Taylor, N. Embaye, Y. Zhe, and J. Zhou, Proc. SPIE **6713**, 671308 (2007).

[24] E. W. Taylor, Proc. SPIE **6713**, 671307 (2007).

[25] I. D. W. Samuel, A. E. Vasdekis, G. Tsiminis, G. A. Turnbull, and E. W. Taylor, Proc. SPIE **6713**, 671304 (2007).

[26] H. Kuhn, J. Chem. Phys. **17**, 1198 (1949).

[27] R. Fork, B. Greene, and C. Shank, Appl. Phys. Lett. **38**, 671 (1981).

[28] F. Duarte and L. Hillman, *Dye Laser Principles, With Applications* (Academic Press, Inc., New York, 1990).

[29] F. Gao, Y. Wang, J. Zhang, D. Shi, M. Wang, R. Humphry-Baker, P. Wang, S. Zakeeruddin, and M. Gratzel, Chem. Commun. **23**, 2635 (2008).

[30] "Ultrathin, dye-sensitized solar cells called most efficient to date," ScienceDaily (2006), www.sciencedaily.com/releases/2006/09/060918201621.htm.

[31] A. Yella, H.-W. Lee, H. N. Tsao, C. Yi, A. K. Chandiran, M. Nazeeruddin, E. W.-G. Diau, C.-Y. Yeh, S. M. Zakeeruddin, and M. Gratzel, Science **334**, 629 (2011).

[32] R. M. Wood, *Laser-Induced Damage of Optical Materials*, Series in Optics and Optoelectronics (Taylor & Francis, Boca Raton, FL, 2003).

[33] G. J. Exarhos, A. H. Guenther, M. R. Kozlowski, and M. J. Soileau, *Laser-Induced Damage in Optical Materials* (SPIE, Bellevue, WA, 1998).

[34] P. White, G. Exarhos, M. Bowden, N. Dixon, and D. Gardiner, J. Mater. Res. **6**, 126 (1991).

[35] J. F. Rabek, *Polymer Photodegradation: Mechanisms and Experimental Methods* (Springer-Science+Business Media, Philadelphia, PA, 1995).

[36] L. Cerdan, A. Costela, G. Duran-Sampedro, I. Garcia-Moreno, M. Calle, M. J. y Seva, J. de Abajo, and G. Turnbull, J. Mater. Chem. **22**, 8938 (2012).

[37] W. Yunus and C. Sheng, Suranaree J. Sci. Technol. **11**, 138 (2004).

[38] C. Fellows, U. Tauber, C. Carvalho, and C. Carvalhaes, Braz. J. Phys. **35**, 933 (2005).

[39] A. Kurian, N. George, B. Paul, V. Nampoori, and C. Vallabhan, Laser Chem. **20**, 99 (2002).

[40] Q. Zhang, M. Canva, and G. Stegeman, Appl. Phys. Lett. **73**, 912 (1998).

[41] M. Mortazavi, H. Yoon, and I. McCulloch, Polym. Prepr. (Am. Chem. Soc., Div. Polym. Chem.) **35**, 198 (1994).

[42] D. G. J. Sutherland, J. A. Carlisle, P. Elliker, G. Fox, T. W. Hagler, I. Jimenez, H. W. Lee, K. Pakbaz, L. J. Terminello, S. C. Williams, F. J. Himpsel, D. K. Shuh, W. M. Tong, J. J. Jia, T. A. Callcott, and D. L. Ederer, Appl. Phys. Lett. **68**, 2046 (1996).

[43] P. Annieta, L. Joseph, L. Irimpan, P. Radhakrishnan, and V. Nampoori (unpublished).

[44] N. Tanaka, N. Barashkov, J. Heath, and W. Sisk, Appl. Opt. **45**, 3846 (2006).

[45] A. Albini, E. Fasani, and S. Pietra, J. Chem. Soc., Perkin Trans 2 **11**, 1393 (1982).

[46] A. Dubois, M. Canva, A. Brun, F. Chaput, and J.-P. Boilot, Appl. Opt. **35**, 3193 (1996).

[47] M. D. Rahn and T. A. King, in *Sol-Gel Optics III,* edited by J. Mackenzie (SPIE Press, Bellingham, WA, 1994) Vol. 2288, p. 382.

[48] D. Avnir, D. Levy, and R. Reisfeld, J. Phys. Chem **88**, 5956 (1984).

[49] E. T. Knobbe, B. Dunn, P. D. Fuqua, and F. Nishida, Appl. Opt. **29**, 2729 (1990).

[50] I. P. Kaminow, L. W. Stulz, E. A. Chandross, and C. A. Pryde, Appl. Opt. **11**, 1563 (1972).

[51] P. L. Chu, Opt. Photonics News **16**, 52 (2005).

[52] R. A. Norwood and G. Khanarian, Electron. Lett. **26**, 2105 (1990).

[53] W. Wang, D. Chen, H. R. Fetterman, W. H. Steier, L. R. Dalton, and P. M. D. Chow, Appl. Phys. Lett. **67**, 1806 (1995).

[54] S. R. Vigil, Z. Zhou, B. K. Canfield, J. Tostenrude, and M. G. Kuzyk, J. Opt. Soc. Am. B **15**, 895 (1998).

[55] B. Howell and M. G. Kuzyk, J. Opt. Soc. Am. B **19**, 1790 (2002).

[56] B. Howell and M. G. Kuzyk, Appl. Phys. Lett. **85**, 1901 (2004).

[57] N. Embaye, S. K. Ramini, and M. G. Kuzyk, J. Chem. Phys. **129**, 054504 (2008).

[58] Y. Zhu, J. Zhou, and M. G. Kuzyk, Opt. Lett. **32**, 958 (2007).

[59] Y. Zhu, J. Zhou, and M. G. Kuzyk, Opt. Photonics News **18**, 31 (2007).

[60] G. D. Peng, Z. Xiong, and P. L. Chu, J. Lightwave Technol. **16**, 2365 (1998).

[61] B. R. Anderson, S. K. Ramini, and M. G. Kuzyk, in *Laser-Induced Damage in Optical Materials*, edited by G. Exarhos (SPIE Press, Bellingham, WA, 2011), Paper no. 81900N.

[62] P. Kobrin, R. Fisher, and A. Gurrola, Appl. Phys. Lett. **85**, 2385 (2004).

[63] L. DesAutels, M. G. Kuzyk, and C. Brewer, Opt. Express **17**, 18808 (2009).

[64] S. K. Ramini and M. G. Kuzyk, J. Chem Phys. **137**, 054705 (2012).

[65] K. D. Singer and L. A. King, J. Appl. Phys. **70**, 3251 (1991).

[66] S. K. Ramini, B. R. Anderson, S. T. Hung, and M. G. Kuzyk, Polym. Chem. **4**, 4948 (2013).

[67] S. K. Ramini, B. R. Anderson, and M. G. Kuzyk, in *SPIE Laser Damage Symposium Proceedings*, edited by G. Exarhos (SPIE Press, Bellingham, WA, 2011), Paper no. 81900P.

[68] D. Duque and P. Tarazona, J. Chem Phys. **107**, 10207 (1997).

[69] P. Collings, A. Dickinson, and E. Smith, Liq. Cryst. **37**, 701 (2010).

[70] M. Cates and S. Candau, J. Phys.: Condens. Matter **2**, 6869 (1990).

[71] C. B. McKitterick, N. L. Erb-Satullo, N. D. LaRacuente, A. J. Dickinson, and P. J. Collings, J. Phys. Chem. B **114**, 1888 (2010).

[72] M. Coopersmith and R. Brout, Phys. Rev. **130**, 2539 (1963).

[73] J. Henderson, J. Chem. Phys. **130**, 045101 (2009).

[74] P. Maiti, Y. Lansac, M. Glaser, and N. Clark, Liq. Cryst. **29**, 619 (2002).

[75] B. Anderson, S. K. Ramini, and M. G. Kuzyk, J. Opt. Soc. Am. B **28**, 528 (2011).

[76] B. R. Anderson, S. T. Hung, and M. G. Kuzyk, in *Nanophotonics and Macrophotonics for Space Environments VI*, edited by E. W. Taylor (SPIE Press, Bellingham, WA, 2012), Vol 8519, 85190H.

[77] B. R. Anderson, S. T. Hung, and M. G. Kuzyk, in *Laser-Induced Damage in Optical Materials: 2012*, edited by G. J. Exarhos,

V. E. Gruzdev, J. A. Menapace, D. Ristau, and M. J. Soileau (SPIE Press, Bellingham, WA, 2012) Vol. 8530, Paper: 85310G.

[78] B. R. Anderson, S.-T. Hung, and M. G. Kuzyk, JOSA B **30**, 3193 (2013).

[79] S. K. Ramini and M. G. Kuzyk, in *Nanophotonics and Macrophotonics for Space Environments VI,* edited by E. W. Taylor (SPIE Press, Bellingham, WA, 2012) Vol. 8519, Paper: 85190G.

[80] M. G. Kuzyk and S. K. Ramini, in *Nanophotonics and Macrophotonics for Space Environments VI*, edited by E. W. Taylor (SPIE Press, Bellingham, WA, 2012) Vol. 8519, Paper: 85190E.

[81] M. G. Kuzyk and S. K. Ramini, in *Laser-Induced Damage in Optical Materials: 2012*, edited by G. J. Exarhos, V. E. Gruzdev, J. A. Menapace, D. Ristau, and M. J. Soileau (SPIE Press, Bellingham, WA, 2012) Vol. 8530, Paper: 853014.

[82] B. Anderson, S.-T. Hung, and M. G. Kuzyk, Opt. Com. **318**, 180 (2014).

[83] B. R. Anderson and M. G. Kuzyk, arXiv:1401.5126 (2014).

[84] B. R. Anderson, E. Bernhardt, and M. G. Kuzyk, in *Optical Processes in Organic Materials and Nanostructures*, edited by R. Jakubiak (SPIE Press, Bellingham, WA, 2012) Vol. 8474, Paper: 84740Y.

[85] J. Kochi, Pure Appl. Chem. **63**, 255 (1991).

[86] B. Cumpston and K. Jensen, Synth. Met. **73**, 195 (1995).

[87] S. L. Li and J. Guillet, Macrmolecules **17**, 41 (1984).

[88] N. J. Dawson, B. R. Anderson, J. L. Schei, and M. G. Kuzyk, Phys. Rev. A **84**, 043406 (2011).

[89] N. J. Dawson, B. R. Anderson, J. L. Schei, and M. G. Kuzyk, Phys. Rev. A **84**, 043407 (2011).

[90] M. Khan, M. Renak, G. Bazan, and Z. Popovic, J. Am. Chem. Soc. **119**, 5344 (1997).

[91] Y. Su, Y. Yang, H. Zhang, Y. Xie, Z. Wu, Y. Jiang, N. Fukata, Y. Bando, and Z. Wang, Nanotechnology **24**, 295401 (2013).

[92] K.-S. Kang, W. Sisk, M. Raja, and F. Farahi, J. Photochem. Photobiol., A **121**, 133 (1999).